The effect of heterogeneities in hydrate saturation on gas production from natural systems

David Riley[a,b], Héctor Marin-Moreno[b] and Tim A. Minshull[a]

[a]*Ocean and Earth Science, University of Southampton, European Way, Southampton SO14 3ZH, UK*

[b]*National Oceanography Centre, University of Southampton Waterfront Campus, European Way, Southampton SO14 3ZH, UK*

Corresponding author email: d.c.riley@soton.ac.uk

Declarations of interest: none

Funding source had no involvement in study design; in the collection, analysis and interpretation of data; in the writing of the report; or in the decision to submit the article for publication.

Highlights

- Hydrate saturation heterogeneity causes gas production rate fluctuations up to ±25%
- 1% heterogeneous hydrate change has equal production effect to 10% homogenous change
- Hydrate-sourced gas avoids migrating through areas of high hydrate saturation
- Hydrate at the dissociation front controls gas production in high permeability layers

Abstract

Understanding the rate and time evolution of gas release from natural gas hydrate systems is important when evaluating the potential of gas hydrate as a future energy source, or the impact of gas from hydrate on climate. The release of gas from hydrate is heavily influenced by a number of factors, many of which vary through the hydrate system. The fundamental heterogeneity of natural gas hydrate systems is often poorly represented in models. Here we simulate depressurisation-induced gas production from a single vertical well in 34 models with heterogeneous 2D distributions of hydrate that include layered, columnar or random configurations and comparable models with homogenous saturation distributions. We found that the temporal evolution of gas production rate follows a consistent trend for all models, but at any time the gas production rate across the models varied by up to ±35% in the first year of production, and by up to ±25% thereafter. The primary control on the gas production rate is the overall amount of hydrate in the system, but local variations in hydrate saturation cause significant fluctuations in the time evolution of production. These hydrate variations can cause changes in the gas flow path through the system and associated drops in gas production rate continuing for multiple years. Overall, our results suggest that small levels of heterogeneity in hydrate systems can cause variations in the gas production rate similar in scale to much larger variations in homogenous systems. Our work provides an error margin for previously modelled gas production rates, and a note of caution for potential commercial development of gas hydrate.

Keywords

Natural gas hydrate; Heterogeneity; Gas production; Numerical simulation; Depressurization

1. Introduction

There is ongoing global interest in the potential development of gas hydrates as an unconventional energy source, to contribute to growing global demand of cleaner fossil fuel resources. Gas hydrates are solid-ice compounds containing molecules of gas, normally methane, within voids in regular crystalline structures (Sloan and Koh, 2007). This structure enables each cubic metre of gas hydrate to contain up to 180 cubic metres of gas at standard pressure and temperature conditions, that can potentially be released through conventional technology, making hydrate an energy-dense fuel source (Sloan, 2003). Gas hydrates form in

hydrocarbon systems at high pressures and low temperatures. Accordingly, natural hydrates are found primarily onshore in permafrost areas and offshore beneath continental slopes and deep waters. In polar areas, because of their low seabed temperatures, hydrate can be found in relatively shallow waters. The global volume of recoverable gas contained within gas hydrates is believed to be comparable in scale to global conventional gas resources (Chong et al., 2016). This abundance has motivated pilot testing of natural gas production from hydrates in prominent markets including Japan, China and the United States (Anderson et al., 2014; Konno et al., 2017; Li et al., 2018).

Numerical simulation of gas production from hydrate reservoirs is used as with conventional resources, to test production schemes and determine the productivity of specific reservoirs. Several simplifications are made when approximating real-world hydrate provinces with numerical models, including the representation of the hydrate-bearing domain. Complex distributions of hydrate are frequently modelled as a homogenous volume (e.g. Kim et al., 2018; Yan et al., 2018; Yu et al., 2018; Zheng et al., 2018), or as a sequence of layers with constant hydrate saturation (e.g. Chen et al., 2018a; Feng et al., 2019; Yuan et al., 2017). Natural systems rarely display this level of homogeneity, as small compositional variations or structural irregularities will alter how hydrate is distributed (Behseresht and Bryant, 2012). Some recent modelling seeks to improve accuracy to the real world by introducing heterogeneity based upon available well data (Ajayi et al., 2018; Jin et al., 2018). However, there has been limited study on how significant modelling assumptions on hydrate saturation are for final production values (Bhade and Phirani, 2015; Nandanwar et al., 2016; Reagan et al., 2010). Techniques for quantifying subsurface hydrate also carry some error (Riedel et al., 2010), so even a perfect model of available data may be subtly different to the real world situation it is representing.

Our chosen model environment is the Alaskan Mount Elbert system, a cold, multi-layered hydrate formation onshore beneath the Prudhoe Bay area of the Alaskan North Slope. We use this site because it has been the subject of hydrate research for almost 50 years (Collett et al., 2011a), has well log data available, and there are published modelling studies with which we can compare our results (Hunter et al., 2011). Previous models suggest that the commercial potential of this hydrate system is low (Moridis et al., 2011). Here we

focus on providing general, process-based insights into the effect of hydrate saturation heterogeneity on gas production and do not seek to optimise the production process. We explore hydrate saturation as it has a direct impact on whether a gas hydrate reservoir is considered a prospective target (Boswell et al., 2015), and also alters the hydrological and thermal response of the system (Tamaki et al., 2017). Our work provides insight into how heterogeneity affects gas production and the associated implications for future hydrate exploitation.

2. Methods

We used the TOUGH+Hydrate simulator for multi-phase fluid and heat transport in gas hydrate bearing media. TOUGH+Hydrate models hydrate dissociation or formation, as a kinetic or equilibrium process, and the associated phase changes amongst four possible phases (gas, liquid, solid-ice, solid-hydrate). We assumed an equilibrium hydrate reaction, as it is less computationally intensive while giving very similar results on our modelling scale (Kowalsky and Moridis, 2007). TOUGH+Hydrate can simulate three production methods or combinations thereof, depressurisation, thermal stimulation or the use of an inhibitor (Moridis, 2008) and has been used extensively in similar hydrate modelling problems, thus validating our approach (Li et al., 2016).

Gas hydrate has been encountered throughout the North Slope in six units (designated A-F), which range from metres to tens of metres thick (Collett, 1993). Our model includes the two hydrate bearing layers that were cored in 2007 (Hunter et al., 2011), C and D, with unit D used as the primary model production target (Figure 1). We have used existing well log data and production simulation parameters as the basis for our modelling (Table 1). Unit D is a 13.4 m thick gas hydrate bearing layer at 616.4 – 627.9 m depth, and unit C is a 16 m gas hydrate bearing layer from 650 – 666 m depth, with some layered structure with significantly lower hydrate saturation than the unit overall (Collett et al., 2011b). Gas hydrate saturation in the layers has been estimated at 50 – 80% from resistivity modelling, acoustic and shear wave velocities and core sampling (Collett et al., 2011b). For our baseline homogeneous model we chose 55% saturation as representative for unit D, and 50% saturation for unit C. We conducted two other homogeneous tests with saturations ±5% from these values. In our heterogeneous models saturation varied between 30 – 70%. We assumed the non-hydrate-bearing layers to be fully aqueous saturated initially.

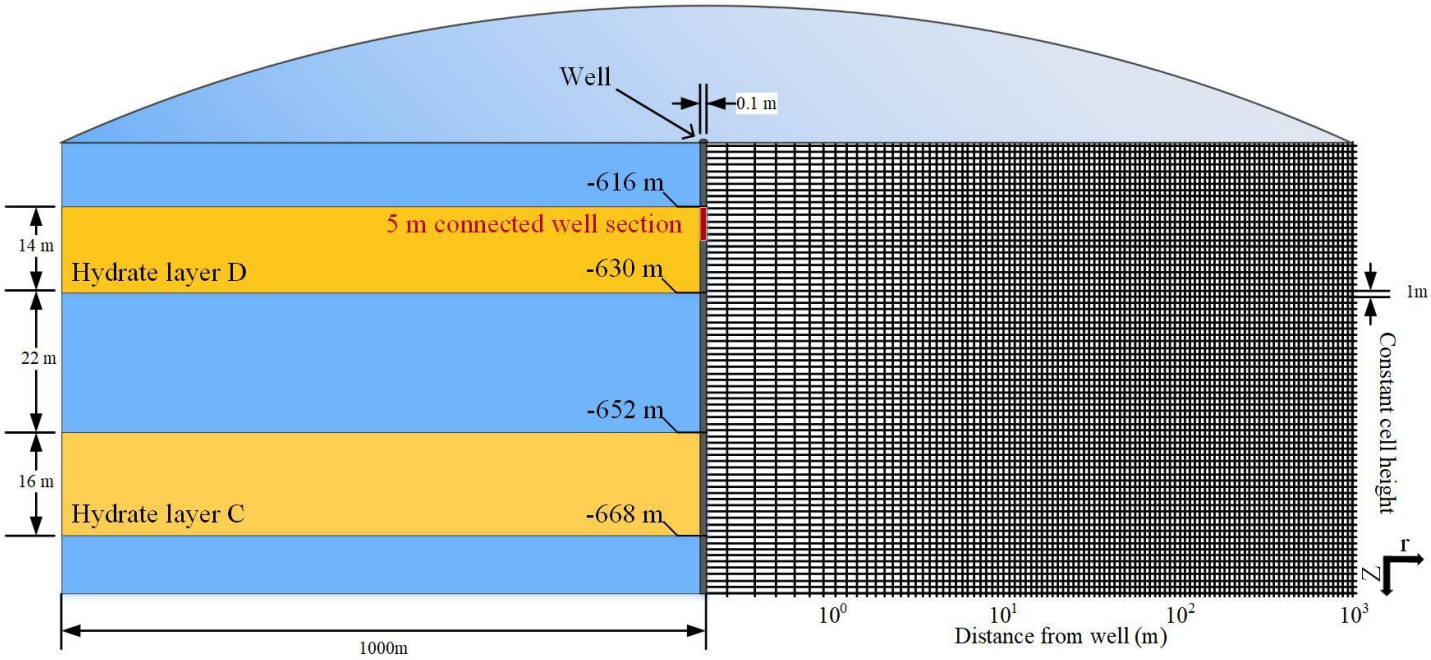

Figure 1: Schematic diagram of our 2D radially symmetric model used (left) and the numerical mesh used (right). Note that the variation in cell size in the radial axis is on a logarithmic scale.

Our model uses an evolving porous medium approach, in which hydrate changes affect the intrinsic permeability of the medium but not the capillary pressure. Relative permeability and capillary pressure are controlled by the equations and parameters given in Table 1. We have used values of these specific parameters that are equal to those used in previous studies on Mt Elbert to allow our results to be compared. We recognise that experimental studies suggest different values for some of these parameters (Mahabadi et al., 2016; Mahabadi and Jang, 2014).

Table 1: Numerical parameters of different layers used in our model

Parameter		Value	Reference
Rock grain density (kg/m^3)		2700	*(Winters et al., 2011)*
Rock grain specific heat (J/kg/C)		1000	*(Anderson et al., 2011)*
Porosity	*Unit D*	0.4	*(Winters et al., 2011)*
	Unit C	0.35	*(Winters et al., 2011)*
	Other lithologies	0.3	*(Winters et al., 2011)*
Isotropic permeability (m^2)	*Unit D*	$1e^{-12}$	*(Winters et al., 2011)*
	Unit C	$7e^{-13}$	*(Winters et al., 2011)*
	Other lithologies	$5e^{-14}$	*(Winters et al., 2011)*
Saturated heat conductivity	*Unit D*	2.20	*(Waite et al., 2009)*
(W/m/C)	*Unit C*	2.50	*(Waite et al., 2009)*
	Other lithologies	2.85	*(Waite et al., 2009)*
Relative permeability	$k_{rA} = max\left\{0, min\left\{\left[\frac{S_A - S_{irA}}{1 - S_{irA}}\right]^n, 1\right\}\right\}$		*(Stone, 1970)*
	$k_{rG} = max\left\{0, min\left\{\left[\frac{S_G - S_{irG}}{1 - S_{irG}}\right]^{n_G}, 1\right\}\right\}$		
S_{irA}		0.20	*(Moridis et al., 2011)*
S_{irG}		0.02	*(Moridis et al., 2011)*
n		4.50	*(Anderson et al., 2011)*
n_G		3.10	*(Anderson et al., 2011)*
Capillary pressure	$P_{cap} = -P_0\left[(S^*)^{-\frac{1}{\lambda}} - 1\right]^{1-\lambda}$, $S^* = \frac{(S_A - S_{irA})}{(S_{mxA} - S_{irA})}$ $-P_{max} \le P_{cap} \le 0$		*(van Genuchten, 1980)*
λ		0.77437	*(Moridis et al., 2011)*
S_{irA}		0.3	*(Anderson et al., 2011)*
$1/P_0$		0.001	
P_{max} (pa)		$1e^5$	
S_{mxA}		1	*(Moridis and Reagan, 2011)*

The model domain is a 2D radial section (r,z) composed of 7622 cells (Figure 1). In the z-axis the model is 72 cells high, each cell being one metre in height. Radially, cell width varies logarithmically from tens of centimetres adjacent to the well, to tens of metres at the maximum model radius, 1000 m away from the well. The well cells have a width of 0.1 m, commensurate with the wellbore radius. The well is represented by a pseudo-medium with high porosity (100% pore space) and a relatively low permeability (≈$1e^{-12}$ m^2).

115 The well is only connected to the formation in the uppermost 5 m of the hydrate bearing layer D (Figure 1)
116 and elsewhere well cells are only connected vertically to other well cells. This configuration simulates a
117 perforated well section in the producing section of the target reservoir as the only exchange point for fluids
118 between the well and its surroundings. We use a relatively low well permeability to reduce the
119 computational cost of each simulation; a necessity for the number of models used in this work. This
120 permeability assumption does not affect our analysis because we measure the gas production rate at the
121 perforated section of the well where gas enters from the reservoir, and not at the top of the well.

122 Our modelling workflow is illustrated in Figure 2. We fix the pressure and temperature conditions at the
123 bottom, top and right boundaries of the model, and the well acts as the left boundary about which the model
124 is radially symmetrical. The 2D simulations were initialised to regional thermal and hydrostatic equilibrium
125 conditions using available data (Hunter et al., 2011; Lee and Collett, 2011, Figure 3). Initial model
126 temperature varies linearly with depth from 2.5 °C to 4 °C, with temperature in unit D between 2.6 and 2.8
127 °C. Unit D pressure increases linearly with depth from 6.7 to 6.8 MPa, with solid hydrate at this temperature
128 beginning dissociation at pressure between 3 to 4 MPa.

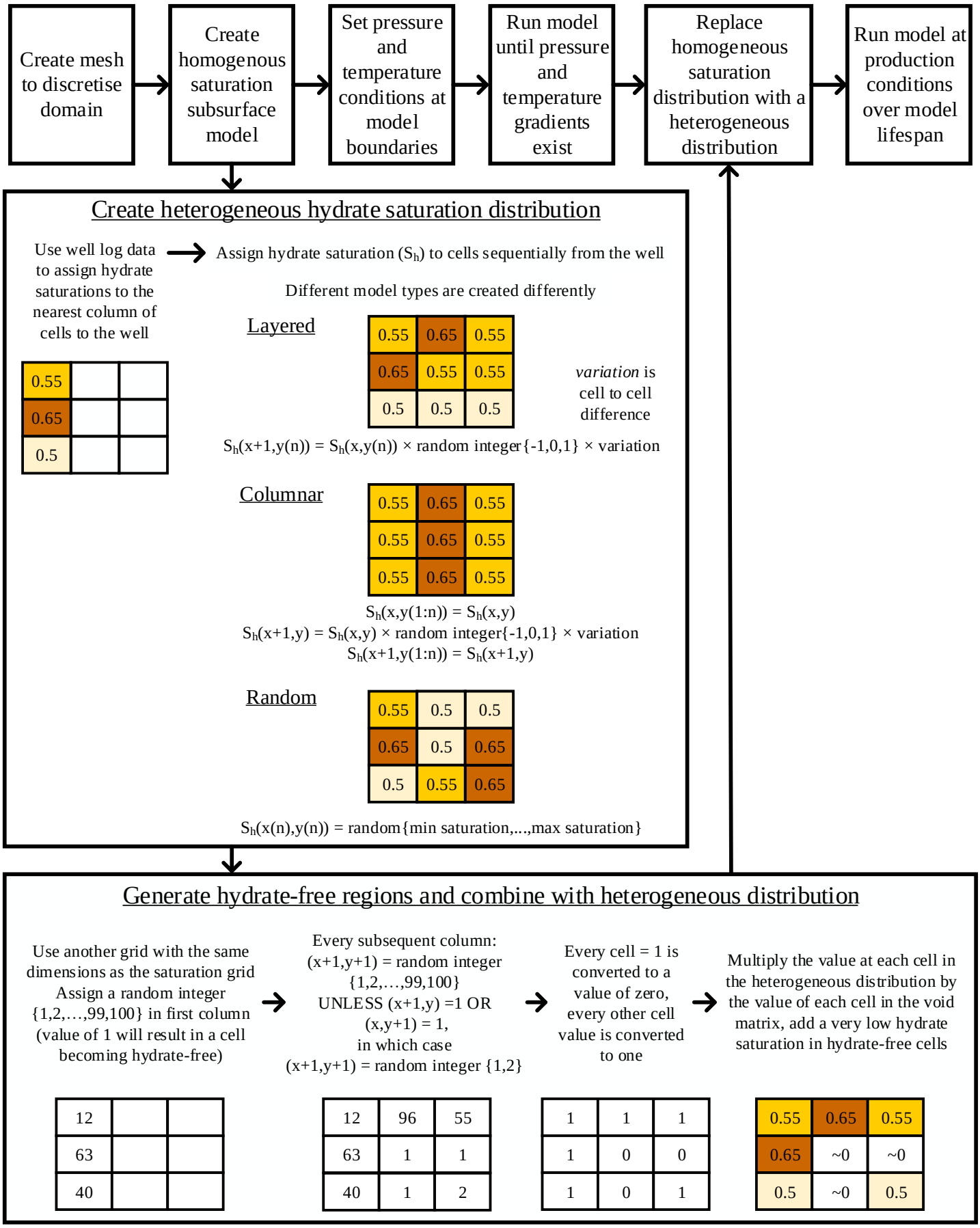

Figure 2: Workflow illustration showing the main stages in model development and the methods used to generate different types of heterogeneous model.

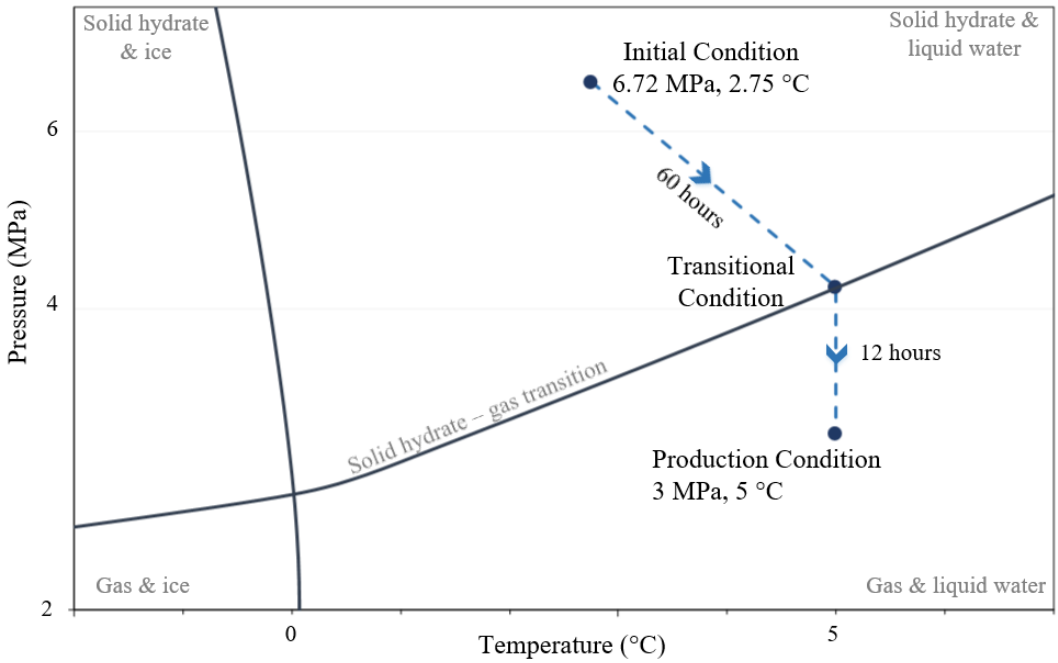

Figure 3: Imposed change in pressure and temperature conditions from initial stable state to production at the well. Pressure axis is logarithmic. Hydrate production conditions were reached by first reducing pressure and increasing temperature over 60 hours (initial to transitional conditions), then by reducing pressure to the production pressure over 12 hours (transitional to production conditions), and finally by maintaining the temperature and pressure at production conditions for 30 years.

We generated 34 heterogeneous models with three classes of hydrate distribution to explore changing this aspect affects gas production rate. Models are broadly classified as layered, columnar or random (Figure 4). The majority of the models used in our study were layered models (n=23, Figure 4a) as natural hydrate is most commonly distributed in layered formations (Cook et al., 2012; Lee and Collett, 2013). To generate layered models, the cells horizontally adjacent to the well margin in the hydrate bearing layers were assigned a hydrate saturation from well log data. For some layered models these saturations were continued unchanged radially across the entire hydrate bearing layer, generating models with constant saturation hydrate layers. In other layered models, saturation in each cell was varied following a random walk from their near-well neighbour cell where the saturation of each subsequent cell in the same layer either increases or decreases by a given amount or stays the same, creating layered models with variation along rows in the radial direction (Figure 2). The variation in the random walk between horizontally neighbouring cells was

set at a constant value of 2.5% or 10% in individual models, to generate models with different degrees of heterogeneity.

We generated fewer columnar and random models as the natural hydrate distributions that these represent are less common in nature than layered formations. Columnar models may represent gas hydrate forming around vertical fluid escape structures (e.g. Lüdmann and Wong, 2003). In columnar models (n=6, Figure 4b), hydrate saturations were allocated to entire columns of cells in each hydrate layer. Values for column saturations were either chosen randomly from the known well log saturation values, or alternatively the well adjacent column was allocated a saturation of 55% and each subsequent column randomly increased or decreased in saturation by 2% or stayed at the same saturation as their near well neighbour column. Random models may represent biogenic hydrate generation, from within the hydrate bearing layer. In fully random models (n=5, Figure 4c) the hydrate saturation of each cell in the hydrate bearing layers was allocated a random saturation from a continuous sample space with a constrained maximum (75%) and minimum (25%) saturation. To add further heterogeneity to all models, hydrate-free regions were seeded in the hydrate bearing layers. Hydrate-free regions were seeded randomly from the well outwards with each individual cell given a 1% chance of being made hydrate-free, unless the near-well neighbour to a cell was a hydrate-free cell as this increased the chance of a cell being randomly seeded as hydrate-free to 50%. This approach created connected hydrate-free regions that represent areas where hydrate may not have formed due to local structural or compositional variations. All models are listed in the supplementary material, Table T1.

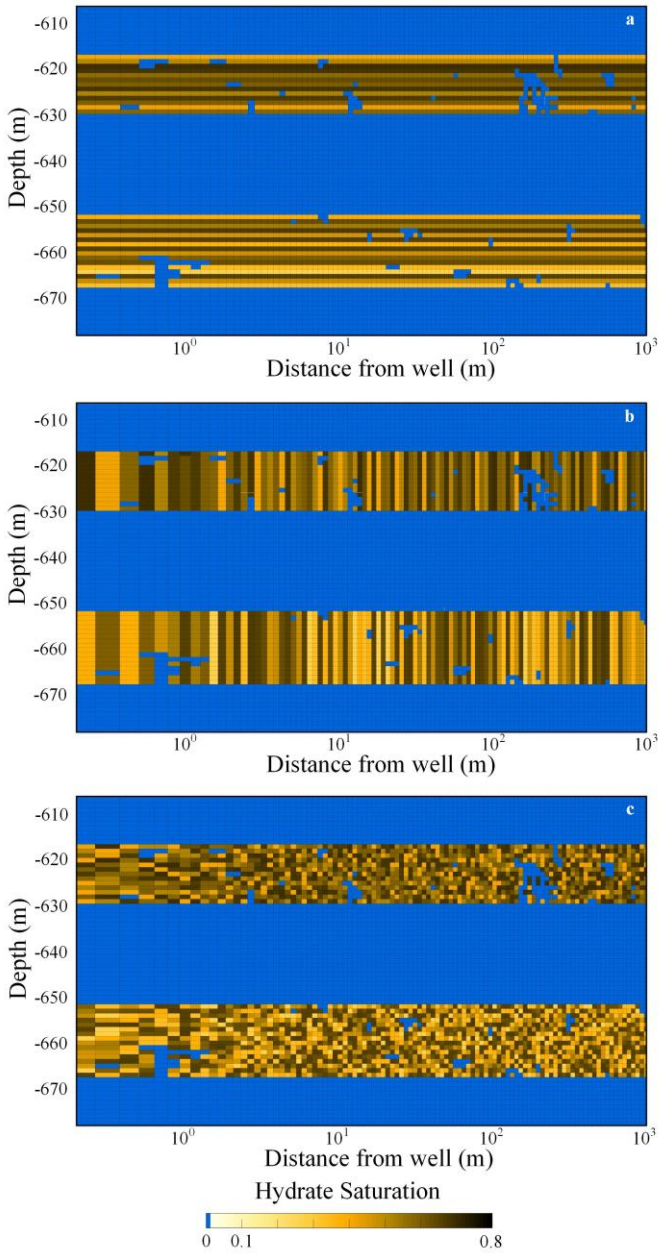

Figure 4: Examples of (a) layered, (b) columnar, and (c) random models of hydrate saturation. Models are in initial state prior to any depressurisation taking place. These models also show connected hydrate-free regions as irregular areas of zero hydrate saturation within the hydrate bearing layers. In all other models the locations of hydrate-free regions were varied. Horizontal scale is logarithmic.

We stimulated hydrate dissociation using depressurisation from a single vertical well. Depressurisation is chosen as the production mechanism as it is seen as the most likely commercial hydrate production method (Demirbas, 2010; Li et al., 2010). We impose a constant bottom-hole pressure of 3 MPa in the connected well section (Figure 1). To reach this pressure we use a two stage pressure drop, initially dropping pressure to the pressure at which dissociation is about to commence, then dropping pressure to the 3 MPa final

condition (Figure 3). This well pressure destabilises solid hydrate under the thermodynamic conditions of our model system, but it is not below the quadruple point pressure, limiting ice formation in the system. Similar to previous modelling studies on depressurisation-induced, hydrate-source gas production at Mt Elbert (Moridis et al., 2011), we imposed a temperature of 5 °C in the connected well section throughout production to promote hydrate dissociation and to counteract partially the endothermic nature of the dissociation process. Our target reservoir at Mt Elbert is only 2 – 3 °C pre-production (Lee and Collett, 2011), meaning heat input is necessary to continue hydrate dissociation, maintain gas flow and prevent ice blockages developing at the interface between the well and the reservoir. The imposed pressure and temperature conditions for production are only fixed in the 5 m well section connected to the formation. Our production scenario was maintained for 30 years to simulate the operational lifespan of a typical gas well. Gas production rate was measured by gas flow into the well. Although also present in the model, unit C was not actively targeted for depressurisation.

We quantified each heterogeneous saturation distribution using a series of summary statistics including the arithmetic mean hydrate saturation, a weighted mean, and a weighted mean considering only the closest half of the model to the well. We applied weighting schemes to the mean to assign less weight to hydrate further from the well and more weight to hydrate that will potentially dissociate. Since we are modelling the effect of heterogeneous hydrate saturation on gas production only material that dissociates or is between dissociating material and the well will influenced the measured gas production at the well. We tested for correlation and potential causation using the Pearson correlation coefficient between each summary statistic and gas production rate at 5 year intervals.

3. Results

We ran 34 heterogeneous models, of which 23 had a layered hydrate configuration, 6 had a columnar hydrate configuration and 5 had a random hydrate configuration and 3 homogeneous hydrate saturation models. All model configurations show similar time evolution of gas production rate (Figure 5). Gas production rate was normalised to the homogeneous 55% hydrate saturation profile to illustrate deviation from this profile. The initial rate of gas production is an instantaneous maximum, double or triple the

standard rate of production in most cases, with variation across all models of ±35% from the homogeneous 55% hydrate saturation model. The initial high rate of production declines by two thirds within the next five years, after which production rate remains between 0.001 and 0.002 Sm^3/s for all models throughout. In the homogeneous models gas production was highest with 60% hydrate saturation and lowest with 50% hydrate saturation (Figure 5). Gas production rate from heterogeneous distributions varies by up to 25% from the homogeneous distribution after the first five years until the end of our simulation (Figure 5). After dropping initially, production rate increases again to a second peak. In all cases a second maximum rate of gas production occurs between 8 to 11 years after production begins (Figure 6). After this second peak, production rate in all scenarios gradual declines towards long-term values of about 0.001 Sm^3/s. Our production rates are similar to those observed for other modelling studies in the same area (e.g. Moridis et al., 2011). Heterogeneous production scenarios on average produce less gas than the homogeneous baseline (Figure 7). The largest variation in gas production rate outside the first year across all models occurs at the same time as the secondary peak in production rate, although this maximum variation is only caused by the behaviour of model 11 (Figure 7). If this model is excluded, the relative difference in gas production rate between all models remains at about 15% from 5 years to the end of production (Figure 5). The time evolution of gas production rate shows the balance between the expansion of the depressurisation front and the increasing distance that the produced gas has to migrate to reach the well. Initial high production rate is caused by dissociation of hydrate directly adjacent to the connected well section, as gas generated can immediately enter the well. This initial stage is where the highest spread in gas production rate is observed, as gas production is only dependent on the cells immediately adjacent to the perforated well section, and the mean saturation for this region can be substantially different between models. A second production rate peak occurs at the optimum balance between expansion of the depressurisation front, increasing hydrate dissociation, and increasing distance for produced gas to migrate to the well.

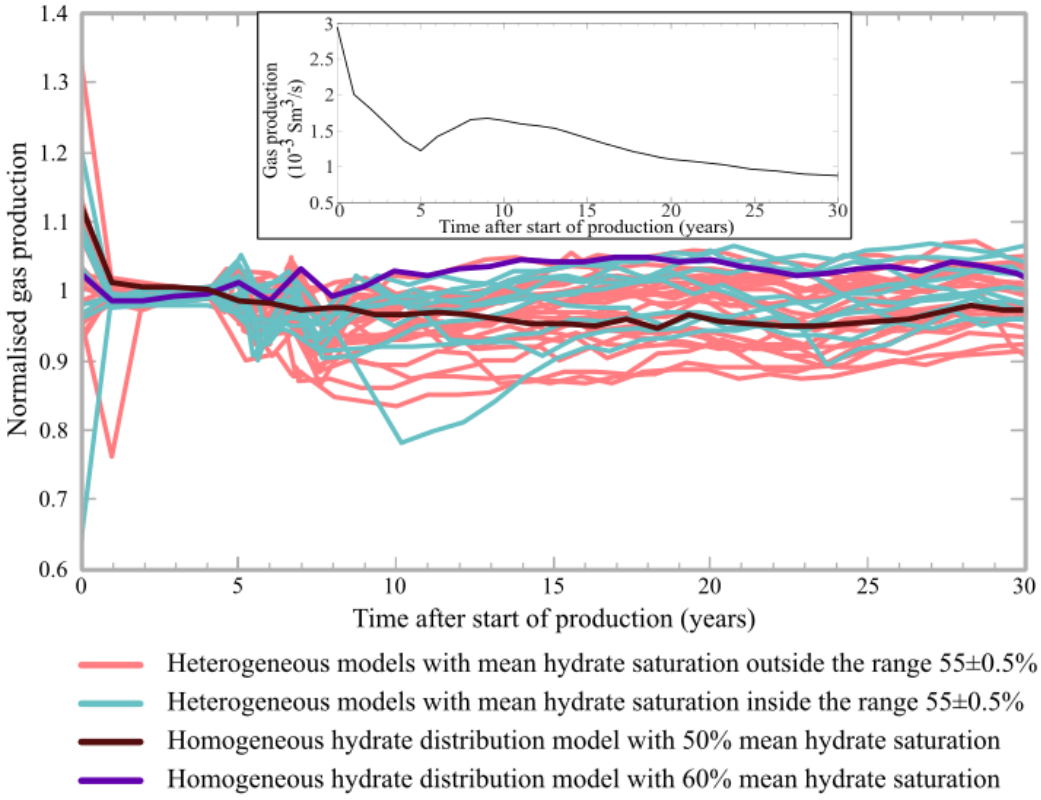

Figure 5: Time evolution of gas production rate at the perforated section of the well for all models normalised to the gas production rate for the homogenous 55% hydrate saturation model (inset).

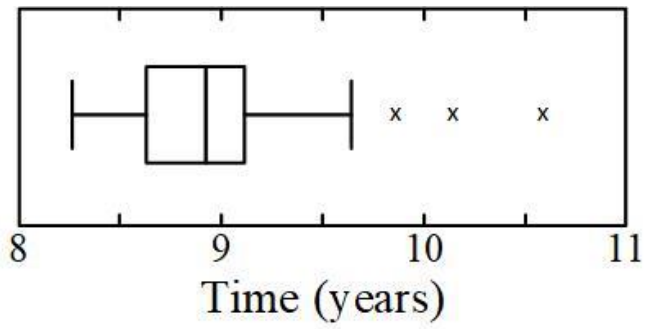

Figure 6: Boxplot of lag time to second production peak across all models. Crosses show outliers, where the time is more than 1.5 times the interquartile range above the upper quartile.

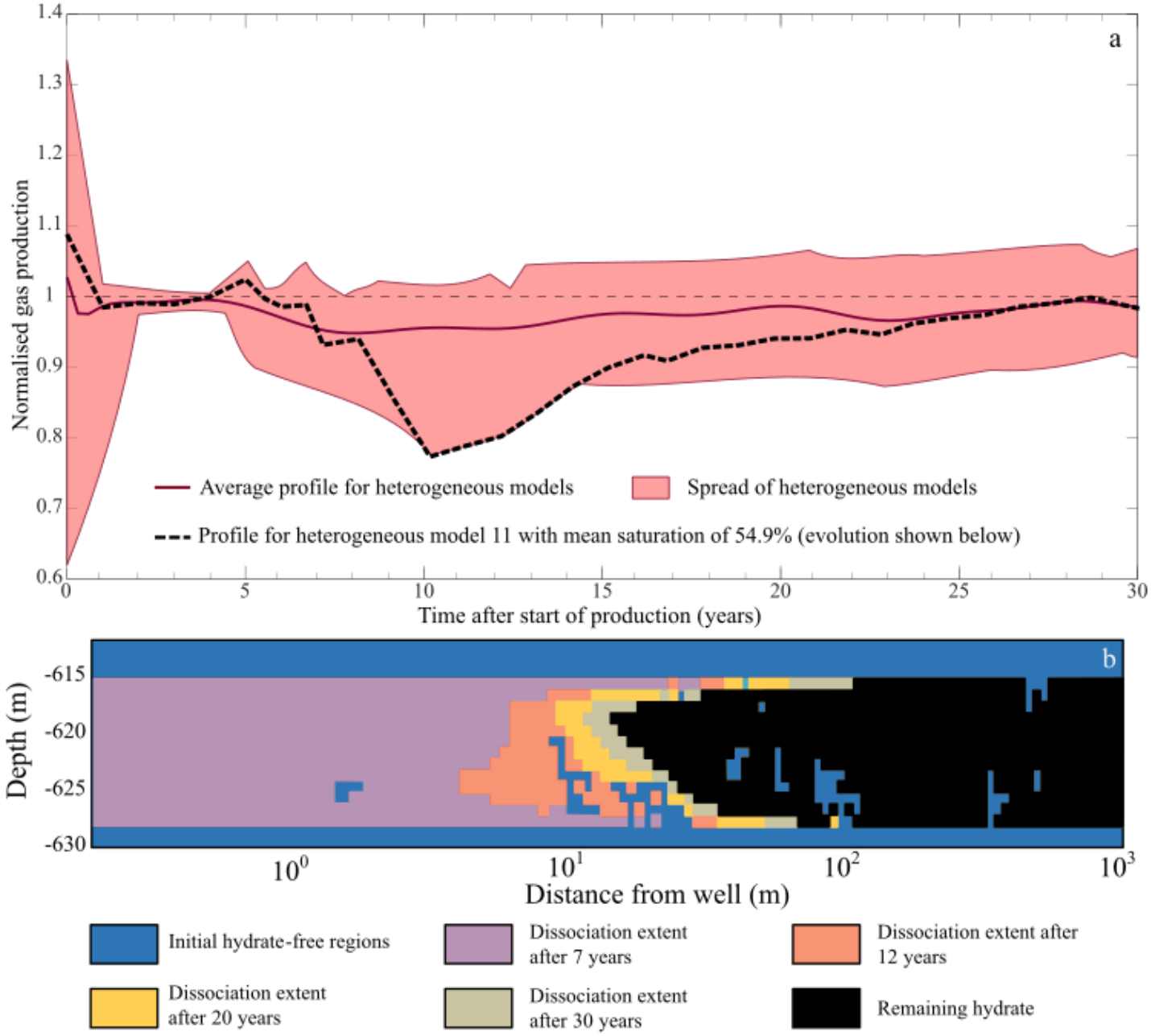

Figure 7: (a) Time evolution of gas production rate at the perforated well section for all heterogeneous hydrate distribution models, normalised to the homogeneous 55% hydrate saturation model. (b) Time evolution of hydrate bearing unit D in heterogeneous model 11 with a mean hydrate saturation of 54.9% over the full production run. Colours indicate new hydrate-free regions at the time indicated, and remaining hydrate after 30 years of production.

The overall pattern of gas production rate is very similar irrespective of the hydrate saturation distribution (Figure 8). Layered models exhibit higher variation in production rate than other distributions due to the higher number of layered models (n=23) compared to columnar (n=6) and random (n=5) models. Random models show gas production rate consistently ≤10% lower than the other two hydrate saturation distributions

primarily because random models contain less hydrate on average (mean hydrate saturation in random models = 46.8%) than other models (mean hydrate saturation in all heterogeneous models = 52.0%,)

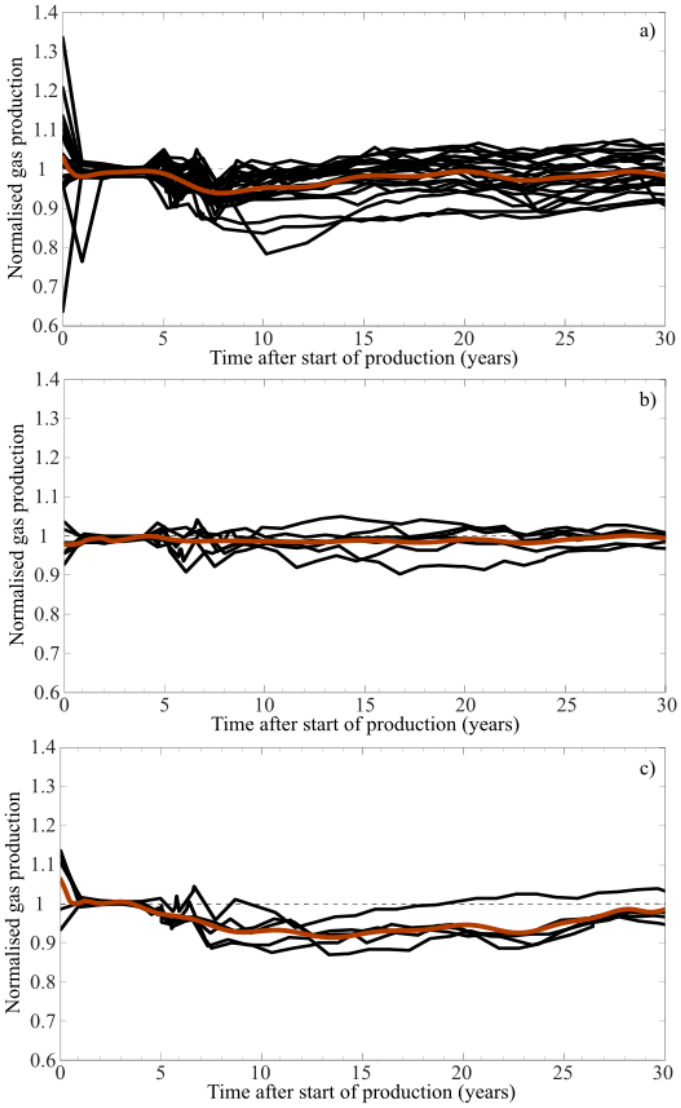

Figure 8: Individually plotted gas production profiles at the perforated section of the well in each heterogeneous a) layered, b) columnar and c) random hydrate distribution model normalised to the homogeneous 55% hydrate saturation model. Red lines show the average gas production rate profile for each model class.

In all models at the end of gas production the dissociation front in unit D has a convex shape resulting from preferential hydrate loss at the top and base of the layer (Figure 7), as this is where heat flux from the surrounding material is the largest (Pooladi-Darvish and Hong, 2011). After 10 years hydrate fully dissociates from the closest ≈10 m to the well, and by the end of 30 years full hydrate dissociation occurs from the next ≈10 m, although the dissociation front extends further radially at the base and especially at the top of unit D, where for some models dissociation occurs across the entire model. The total penetration

depth of the dissociation front and distance is closely similar for all models. This indicates that in our models penetration depth of dissociation is primarily controlled by the depressurisation conditions, and is mostly independent of hydrate saturation.

There is a moderate positive correlation between initial mean hydrate saturation and gas production rate throughout, ($0.5< r <0.67$, $p<0.005$, Figure 7), with the strongest correlation at 15 and 20 years ($0.66< r <0.69$, $p<0.005$, Figure 7). Moderate to high positive correlations between mean saturation and gas production rate indicate that increasing the amount of hydrate in the system increases gas production rate. More hydrate available to dissociate contains a greater volume of trapped gas, which can be released to give a higher production rate over time. When separated by configuration, layered models show similar correlation strengths in a similar pattern to the overall trend (Figure 9), indicating that layered models dominate the overall correlations as they comprise a significant proportion of the overall total of models. The correlations calculated for columnar models alone are not significant ($P>0.005$) due to the small number of columnar models. At some times the correlation for random models is significant, but the same general trend is observed for random models as layered and there are significantly fewer random models so these contribute less than the layered models to the overall trend. The weighting scheme increases the strength of correlation ($0.53< r <0.78$, $p<0.005$, Figure 9). In an attempt to further improve the correlation, and using the fact that penetration depth is similar across all models, we also applied a weighting only using the closest half of the model to the well, as this region approximately encompasses the part of the model which experiences hydrate dissociation due to depressurisation. The result of this second weighting scheme gives a slight further increase to the strength of the correlation ($0.53< r <0.82$, $p<0.005$, Figure 9). This correlation does not consider the contributions to gas production that occur from outside the closest half of the model to the well, especially within the last ten years of production. All correlation summary statistics are presented in the supplementary material, Table T2.

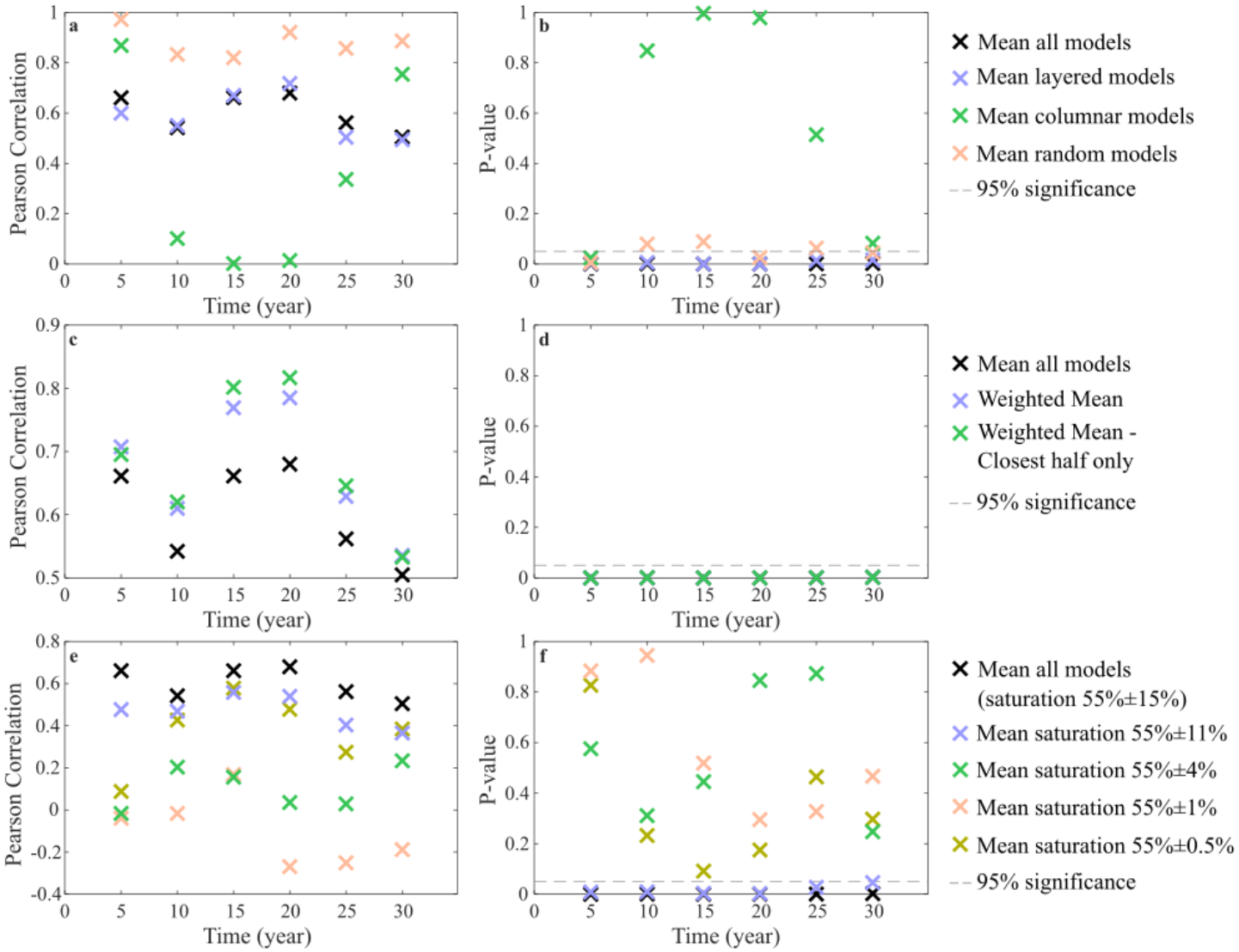

Figure 9: Correlation and confidence values between different estimates of mean hydrate saturation and gas production rate at the perforated section of the well for different model samples. (a) Correlation and (b) confidence values between mean hydrate saturation and gas production rate for the three classes of heterogeneous hydrate distribution models considered. (c) Correlation and (d) confidence values between different estimations of mean hydrate saturation and gas production rate for all heterogeneous hydrate distribution models. (e) Correlation and (f) confidence values between mean hydrate saturation and gas production rate for all heterogeneous hydrate distribution models grouped into five different sampling sets. In (c) symbols plot on top of each other.

4. Discussion

The number of models and their degrees of variation in hydrate mean saturation and distribution are sufficient to identify, but not precisely quantify, impacts from these two parameters independently, as we varied hydrate mean saturation and distribution in our heterogeneous hydrate models concurrently. For

292 further analysis we have divided the total range of models into classes based upon the difference between
293 model hydrate mean saturation and the 55% mean hydrate saturation used in our initial homogenous model.
294 In this way we isolate the impact from hydrate distribution by considering differences in production for all
295 models with similar mean hydrate saturations. By separating the models based upon their mean hydrate
296 saturation, reliable moderate to high correlations between initial means and gas production rates only
297 emerge at all times when reaching variations in saturation of ±11% from the homogenous distribution
298 (Figure 9e, f). This observation suggests that mean hydrate saturation is not the only influence on gas
299 production rate, and is only the primary influence when total hydrate saturation differs significantly
300 between models. For all other groups and times we obtain low or non-significant correlations (Figure 9e, f),
301 likely suggesting that system heterogeneity is causing the observed variations in gas production rate.
302 Sampling all of the heterogeneous production scenarios with mean hydrate saturations of 55±0.5%
303 irrespective of model type (layered, columnar and homogeneous) shows that the scale of variation in gas
304 production rate is larger than between homogeneous distributions with saturations of 55±5% (Figure 5). This
305 result suggests that large local differences in hydrate saturation, which are masked when considering the
306 volume as a whole, can generate significant variations in gas production rate. Therefore, using a range of
307 homogeneous distributions to estimate error may not be sufficient to encompass the variation in gas
308 production rate resulting from natural hydrate distribution heterogeneity.

309 The lag between production initialisation and peak production rate as identified before (e.g. Anderson et al.,
310 2011), is likely caused by the high water production in hydrate dissociation. Excess water must be removed
311 before gas is produced and also requires free gas in the system to build until it becomes a mobile phase
312 (Walsh et al., 2009). The lag to maximum production has been shown to be mesh dependent (Boswell et al.,
313 2017), but this factor will influence the overall lag times exhibited by all models, and cannot explain the
314 differences in lag times shown in this study between models using the same mesh. In our models,
315 differences in hydrate saturation cause variations in free water content, liquid and gas permeabilities,
316 sediment thermal conductivity, and the volume of water produced from hydrate dissociation. The
317 combination of these factors causes the variability in lag times between our models (Figure 6). Over time the
318 propagation rate of the dissociation front in the radial direction decreases as a lower absolute pressure

decrease due to depressurisation at the well is experienced at greater distances from the well. Additionally, the produced gas has to migrate further over time to reach the wellbore. Both factors result in a gradual decline in gas production rate in all models after the first 10 years of production. In a commercial development several production wells may be used with a well spacing lower than the 1 km radial distance of our model (Wilson et al., 2011). Closer well spacing would reduce the migration distance for any produced gas and also contribute to pressure reduction, if depressurisation is applied at different production wells, reducing the decay in gas production over time. By imposing constant depressurisation conditions we do not include the impact of suspensions in depressurisation that would necessarily occur in production and may cause hydrate reformation. However, the focus of our work is comparing dissociation in different hydrate deposits and not attempting to optimise production approaches.

The layers above and below unit D are not modelled here as totally impermeable as assumed in some prior modelling studies (e.g. Chejara et al., 2013; Moridis et al., 2011). We observe that depressurisation propagates into the lower hydrate bearing layer, unit C, causing gas production at the top of unit C, despite our model not directly targeting the layer for production. Gas produced from unit C has to migrate slowly through the lower permeability material between the two hydrate bearing layers before it contributes to production. This contribution begins ≈10 years after production starts. Before this time pressure driven gas flow dominates over buoyancy driven flow and so some gas generated from unit D is driven by pressure into the layer beneath, between units C and D. Gas saturations in the material between the two hydrate bearing layers, with gas contributed from both hydrate bearing layers, reach 10% after 30 years (Figure 10 and supplementary material Video V1). The contribution of non-targeted units is an important consideration when producing hydrate from layered formations. Also, the permeable overburden does not perfectly seal the system, resulting in a fraction of produced gas entering the overburden and not contributing to production. There is no ready pathway for gas escape from the overburden, so gas saturations can reach 15% compared to 5-10% in the hydrate bearing layer. The permeability of the overburden is especially significant as hydrate dissociation propagates preferentially along the top surface of unit D, from where produced gas can immediately enter the overburden. In commercial production the fluid connected region of the well to the formation may need expansion into the overburden to capture this escaped gas.

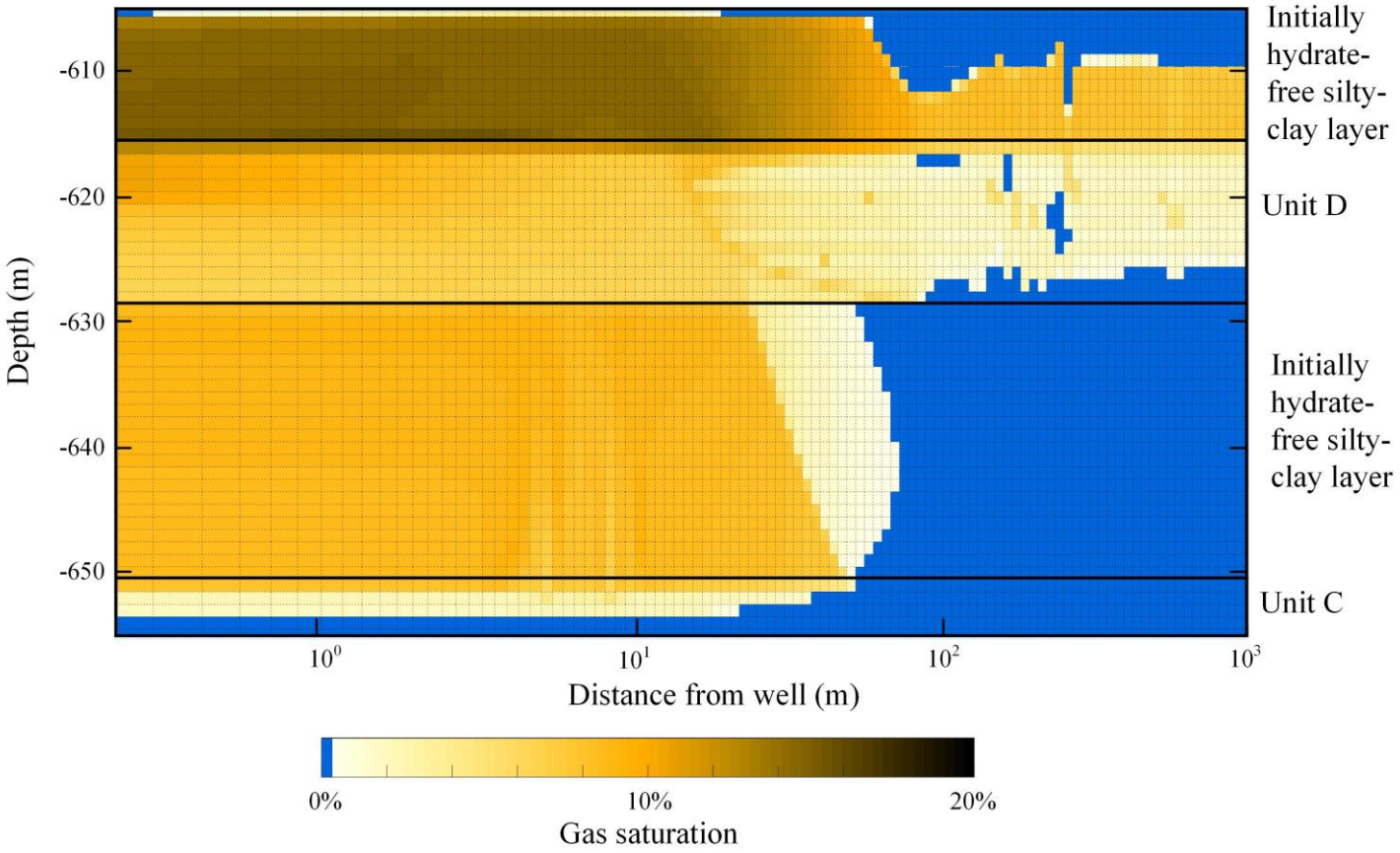

Figure 10: Gas saturation in the layered hydrate model shown in Figure 4a after 30 years of production.

When the dissociation front encounters a hydrate-free region, the deficiency leads to a drop in gas production rate while the hydrate-free region forms part of the active system. The hydrate-free region may promote dissociation further from the well as the pressure wave propagates more easily in the hydrate-free region. In this case however, increasing the range of dissociation does not necessarily increase gas production rate, as gas produced from additionally affected hydrate has further distance to migrate to reach the well. Heterogeneous model 11 (Figure 7) shows effects of both mean hydrate saturation and hydrate distribution. Heterogeneous model 11 is a layered model with a mean saturation (54.9%) that is close to the mean saturation of the initial homogeneous model (55%) but hydrate distribution, and specifically the presence of a large hydrate-free region in the active zone of the hydrate-bearing layer caused a 5 year period where gas production rate is 15% below the average production profile for heterogeneous models (Figure 7a). Before the dissociation front reached this hydrate-free region, and once dissociation has passed this hydrate-free region, gas production rate has a normalised value of 1 (Figure 7a), indicating a gas production rate near-identical to that of the homogeneous model with near-identical hydrate saturation. The hydrate-

bearing layer of our studied system has a very high permeability (10^{-12} m^2), allowing the migration of produced gas to the well to outpace the propagation rate of the dissociation front, and lowering the chance for secondary hydrate reformation. As such, the production rate is mainly controlled by the presence or absence of hydrate at the dissociation front at any given time. Accordingly, regions with significant saturation variation in similar natural systems can cause multi-year periods of irregular gas production rates compared to expected estimates from equivalent homogeneous models.

Gas flow in our model generates pathways preferentially avoiding high hydrate saturation regions which have relatively low permeability. The overall high permeability of our modelled hydrate-bearing layer allows ready creation of fluid pathways around any high hydrate saturation regions acting as temporary barriers. This can lead to isolated regions without gas within the hydrate bearing layer as a result of local high hydrate saturation conditions (Figures 10 and 11 and supplementary material Video V1). Due to preferential hydrate dissociation along the top surface of unit D, gas is present across the width of the model, but not through the entire depth of the hydrate layer. In Figure 11a gas generated at the top of unit D has travelled down to a hydrate-free region within the layer, and then preferentially towards the well using the low hydrate saturation layers at the top of unit D and at 620 m depth, avoiding high hydrate saturation regions. By contrast, in Figure 11b a series of high hydrate saturation layers provides a more effective barrier to gas flow that also explains the lower gas production rate in heterogeneous model 11 over the period 10 - 15 years after gas production begins. Compared to the model in Figure 11a, gas generated at the top of unit D has to migrate deeper into unit D before it finds a lower saturation pathway at 622 m to migrate to the well. Figure 11b also shows the impact of radial variation of hydrate saturation within a broadly layered model, as gas follows the layer at 620 m depth, until increasing hydrate saturation decreases permeability sufficiently to hinder gas flow. In layered hydrate distributions, low hydrate saturation layers provide pathways for lateral flow of gas until a radial change in hydrate saturation occurs. The hydrate-free regions in our domain provide routes for gas to transfer between layers as gas seeks the highest permeability pathway available. Therefore, the path taken for generated gas to reach the well is likely more tortuous the more irregular the hydrate distribution is. Real-world formations also have heterogeneity in a third dimension not represented in our model further complicating the available pathways for gas flow.

Independent validation of our results would be provided by using a geologically equivalent laboratory sample to our modelled reservoir, creating different distributions of synthetic hydrate in this material, then measuring gas generation for imposed dissociation on these hydrate distributions. Further modelling could establish if our conclusions hold when modelling dissociation in other hydrate reservoirs.

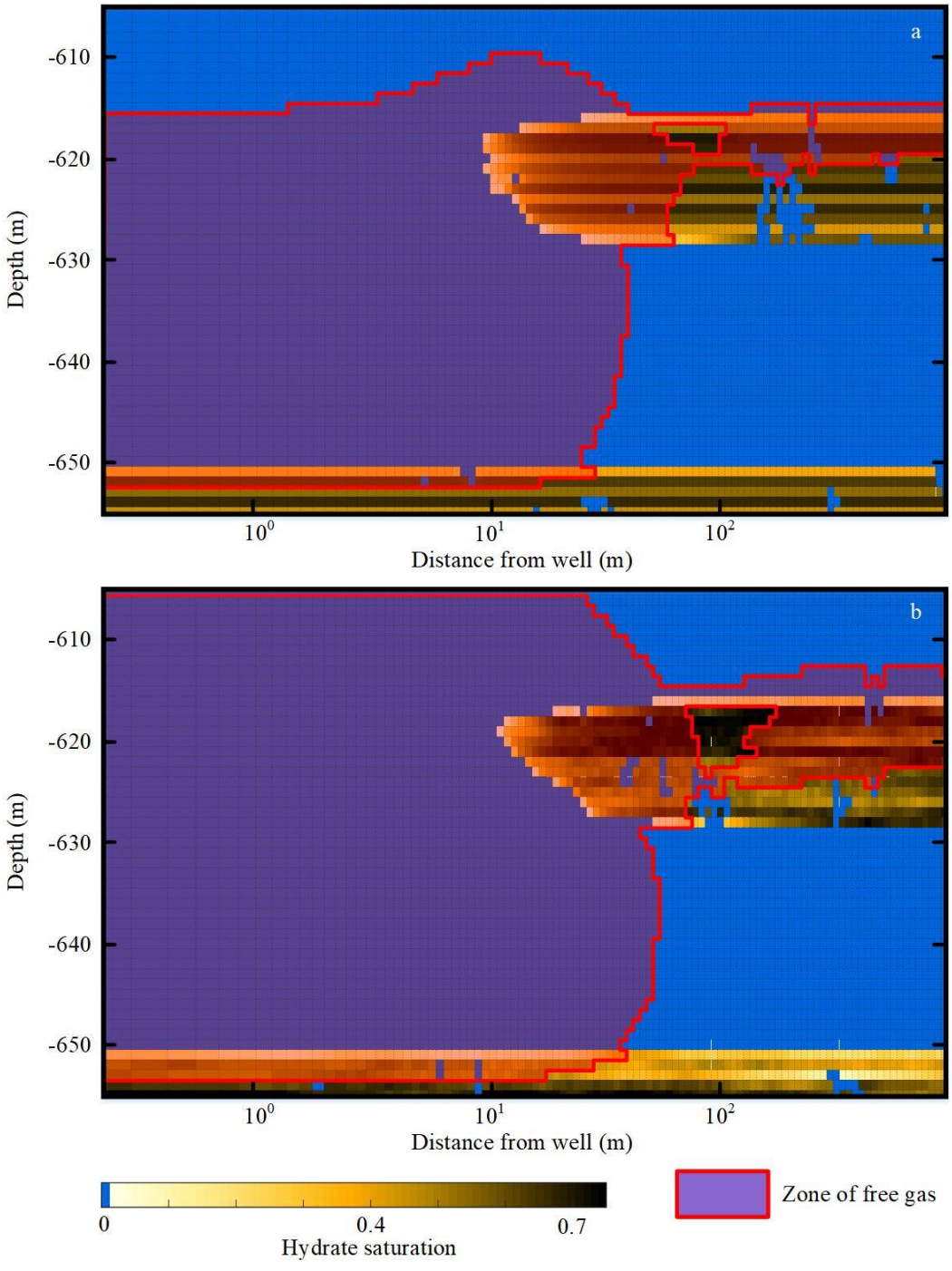

Figure 11: Hydrate and gas saturations for (a) the layered model shown in Figure 4a after 11 years of production and (b) the heterogeneous layered model 11 (gas production rate profile shown in Figure 7a) after 11 years of production.

5. Conclusions

We have used the Mt Elbert site to generate heterogeneous distributions of gas hydrate and assess their impacts on gas migration through the system and gas production rate with respect to homogeneous distributions. The conclusions of our analysis are as follows:

- The general evolution over time of the production profile is similar irrespective of the hydrate distribution but gas production rate can vary by up to ±40% during the first year of production and by up to ±20% over the remaining production lifespan.
- Differences in mean hydrate saturation between models heavily influence gas production rate in active systems when differences in mean hydrate saturation between modelled systems exceed 10%.
- For differences in mean hydrate saturation below 10%, hydrate distribution likely dominates gas production rate variation as the scale of variation in gas production rate between models is larger in models with heterogeneous distributions of hydrate than with homogenous distributions for the same hydrate saturation range.
- In high permeability systems the instantaneous gas production rate is primarily affected by the amount of hydrate at the dissociation front, suggesting that gas production in these systems has little memory of the propagation history of the dissociation front.
- Highly heterogeneous distributions of hydrate, including hydrate-free regions, likely generate a more tortuous migration pathway of generated gas to the well.
- Local large variations in hydrate saturation, such as hydrate-free regions, can be unnoticed when characterizing the whole hydrate layer, particularly when the hydrate-free region is beyond the immediate vicinity of the production well, but can affect gas flow in the formation and production rate for multiple years.
- Heterogeneity in hydrate saturation, results in uncertainty that must be accounted for when attempting to predict gas production from real world gas hydrate deposits.

Author Contributions

Methodology: D.R. and H.M.-M.; Simulations: D.R.; Formal analysis: D.R. and H.M.-M.; Supervision: H.M.-M.; Writing original draft: D.R.; Writing, reviewing and editing: D.R., H.M.-M. and T.M.

Acknowledgements

The authors would like to thank the three anonymous reviewers for their insightful and constructive comments.

Parties interested in acquiring the data presented in this work should contact the lead author. David Riley was supported by the University of Southampton, and a SMMI Leverhulme Trust Doctoral Scholarship. Tim Minshull was supported by a Wolfson Research Merit Award.

References

Ajayi, T., Anderson, B.J., Seol, Y., Boswell, R., Myshakin, E.M., 2018. Key aspects of numerical analysis of gas hydrate reservoir performance: Alaska North Slope Prudhoe Bay Unit "L-Pad" hydrate accumulation. J. Nat. Gas Sci. Eng. 51, 37–43. https://doi.org/10.1016/j.jngse.2017.12.026

Anderson, B.J., Boswell, R., Collett, T.S., Farrell, H., Ohtsuki, S., White, M., Zyrianova, M.V., 2014. Review of the findings of the Ignik Sikumi CO2-CH4 gas hydrate exchange field trial. Presented at the 8th International Conference on Gas Hydrates (ICGH8-2014), Beijing, China.

Anderson, B.J., Kurihara, M., White, M.D., Moridis, G.J., Wilson, S.J., Pooladi-Darvish, M., Gaddipati, M., Masuda, Y., Collett, T.S., Hunter, R.B., Narita, H., Rose, K., Boswell, R., 2011. Regional long-term production modeling from a single well test, Mount Elbert Gas Hydrate Stratigraphic Test Well, Alaska North Slope. Mar. Pet. Geol. 28, 493–501. https://doi.org/10.1016/j.marpetgeo.2010.01.015

Behseresht, J., Bryant, S.L., 2012. Sedimentological control on saturation distribution in Arctic gas-hydrate-bearing sands. Earth Planet. Sci. Lett. 341–344, 114–127. https://doi.org/10.1016/j.epsl.2012.06.019

Bhade, P., Phirani, J., 2015. Gas production from layered methane hydrate reservoirs. Energy 82, 686–696. https://doi.org/10.1016/j.energy.2015.01.077

Boswell, R., Collett, T.S., Myshakin, E., Ajayi, T., Seol, Y., 2017. The increasingly complex challenge of gas hydrate reservoir simulation. Presented at the 9th International Conference on Gas Hydrates, Denver, CO.

Boswell, R., Shipp, C., Reichel, T., Shelander, D., Saeki, T., Frye, M., Shedd, W., Collett, T.S., McConnell, D.R., 2015. Prospecting for marine gas hydrate resources. Interpretation 4, SA13–SA24. https://doi.org/10.1190/INT-2015-0036.1

Chejara, A., Kvamme, B., Vafaei, M.T., Jemai, K., 2013. Simulations of long term methane hydrate dissociation by pressure reduction using an extended RetrasoCodeBright simulator. Energy Convers. Manag. 68, 313–323. https://doi.org/10.1016/j.enconman.2012.09.003

Chen, L., Feng, Y., Kogawa, T., Okajima, J., Komiya, A., Maruyama, S., 2018. Construction and simulation of reservoir scale layered model for production and utilization of methane hydrate: The case of Nankai Trough Japan. Energy 143, 128–140. https://doi.org/10.1016/j.energy.2017.10.108

Chong, Z.R., Yang, S.H.B., Babu, P., Linga, P., Li, X.-S., 2016. Review of natural gas hydrates as an energy resource: Prospects and challenges. Appl. Energy 162, 1633–1652. https://doi.org/10.1016/j.apenergy.2014.12.061

Collett, T.S., 1993. Natural gas hydrates of the Prudhoe Bay and Kuparuk River area, North Slope, Alaska. Am. Assoc. Pet. Geol. Bull. 77, 20.

Collett, T.S., Lee, M.W., Agena, W.F., Miller, J.J., Lewis, K.A., Zyrianova, M.V., Boswell, R., Inks, T.L., 2011a. Permafrost-associated natural gas hydrate occurrences on the Alaska North Slope. Mar. Pet. Geol. 28, 279–294. https://doi.org/10.1016/j.marpetgeo.2009.12.001

Collett, T.S., Lewis, R.E., Winters, W.J., Lee, M.W., Rose, K.K., Boswell, R.M., 2011b. Downhole well log and core montages from the Mount Elbert Gas Hydrate Stratigraphic Test Well, Alaska North Slope. Mar. Pet. Geol. 28, 561–577. https://doi.org/10.1016/j.marpetgeo.2010.03.016

Cook, A.E., Anderson, B.I., Rasmus, J., Sun, K., Li, Q., Collett, T.S., Goldberg, D.S., 2012. Electrical anisotropy of gas hydrate-bearing sand reservoirs in the Gulf of Mexico. Mar. Pet. Geol. 34, 72–84. https://doi.org/10.1016/j.marpetgeo.2011.09.003

Demirbas, A., 2010. Methane hydrates as potential energy resource: Part 2 – Methane production processes from gas hydrates. Energy Convers. Manag. 51, 1562–1571. https://doi.org/10.1016/j.enconman.2010.02.014

Feng, Y., Chen, L., Suzuki, A., Kogawa, T., Okajima, J., Komiya, A., Maruyama, S., 2019. Numerical analysis of gas production from layered methane hydrate reservoirs by depressurization. Energy 166, 1106–1119. https://doi.org/10.1016/j.energy.2018.10.184

Hunter, R.B., Collett, T.S., Boswell, R., Anderson, B.J., Digert, S.A., Pospisil, G., Baker, R., Weeks, M., 2011. Mount Elbert Gas Hydrate Stratigraphic Test Well, Alaska North Slope: Overview of scientific and technical program. Mar. Pet. Geol. 28, 295–310. https://doi.org/10.1016/j.marpetgeo.2010.02.015

Jin, G., Lei, H., Xu, T., Xin, X., Yuan, Y., Xia, Y., Juo, J., 2018. Simulated geomechanical responses to marine methane hydrate recovery using horizontal wells in the Shenhu area, South China Sea. Mar. Pet. Geol. 92, 424–436. https://doi.org/10.1016/j.marpetgeo.2017.11.007

Kim, A.R., Kim, J.T., Cho, G.C., Lee, J.Y., 2018. Methane Production From Marine Gas Hydrate Deposits in Korea: Thermal-Hydraulic-Mechanical Simulation on Production Wellbore Stability. J. Geophys. Res. Solid Earth 123, 9555–9569. https://doi.org/10.1029/2018JB015875

Konno, Y., Fujii, T., Sato, A., Akamine, K., Naiki, M., Masuda, Y., Yamamoto, K., Nagao, J., 2017. Key Findings of the World's First Offshore Methane Hydrate Production Test off the Coast of Japan: Toward Future Commercial Production. Energy Fuels 31, 2607–2616. https://doi.org/10.1021/acs.energyfuels.6b03143

Kowalsky, M.B., Moridis, G.J., 2007. Comparison of kinetic and equilibrium reaction models in simulating gas hydrate behavior in porous media. Energy Convers. Manag. 48, 1850–1863. https://doi.org/10.1016/j.enconman.2007.01.017

Lee, M.W., Collett, T.S., 2013. Scale-dependent gas hydrate saturation estimates in sand reservoirs in the Ulleung Basin, East Sea of Korea. Mar. Pet. Geol. 47, 195–203. https://doi.org/10.1016/j.marpetgeo.2012.09.004

Lee, M.W., Collett, T.S., 2011. In-situ gas hydrate hydrate saturation estimated from various well logs at the Mount Elbert Gas Hydrate Stratigraphic Test Well, Alaska North Slope. Mar. Pet. Geol. 28, 439–449. https://doi.org/10.1016/j.marpetgeo.2009.06.007

Li, G., Moridis, G.J., Zhang, K., Li, X.-S., 2010. Evaluation of Gas Production Potential from Marine Gas Hydrate Deposits in Shenhu Area of South China Sea. Energy Fuels 24, 6018–6033. https://doi.org/10.1021/ef100930m

Li, J., Ye, J., Qin, X., Qiu, H., Wu, N., Lu, Hai-long, Xie, W., Lu, J., Peng, F., Xu, Z., Lu, C., Kuang, Z., Wei, J., Liang, Q., Lu, Hong-feng, Kou, B., 2018. The first offshore natural gas hydrate production test in South China Sea. China Geol. 1, 5–16. https://doi.org/10.31035/cg2018003

Li, X.-S., Xu, C.-G., Zhang, Y., Ruan, X.-K., Li, G., Wang, Y., 2016. Investigation into gas production from natural gas hydrate: A review. Appl. Energy 172, 286–322. https://doi.org/10.1016/j.apenergy.2016.03.101

Lüdmann, T., Wong, H.K., 2003. Characteristics of gas hydrate occurrences associated with mud diapirism and gas escape structures in the northwestern Sea of Okhotsk. Mar. Geol. 201, 269–286. https://doi.org/10.1016/S0025-3227(03)00224-X

Mahabadi, N., Jang, J., 2014. Relative water and gas permeability for gas production from hydrate-bearing sediments. Geochem. Geophys. Geosystems 15, 2346–2353. https://doi.org/10.1002/2014GC005331

Mahabadi, N., Zheng, X., Jang, J., 2016. The effect of hydrate saturation on water retention curves in hydrate-bearing sediments. Geophys. Res. Lett. 43, 4279–4287. https://doi.org/10.1002/2016GL068656

Moridis, G., 2008. TOUGH+Hydrate v1.0 User's Manual: A Code for the Simulation of System Behavior in Hydrate-Bearing Geologic Media. Lawrence Berkeley Natl. Lab.

Moridis, G.J., Reagan, M.T., 2011. Estimating the upper limit of gas production from Class 2 hydrate accumulations in the permafrost: 1. Concepts, system description, and the production base case. J. Pet. Sci. Eng. 76, 194–204. https://doi.org/10.1016/j.petrol.2010.11.023

Moridis, G.J., Silpngarmlert, S., Reagan, M.T., Collett, T., Zhang, K., 2011. Gas production from a cold, stratigraphically-bounded gas hydrate deposit at the Mount Elbert Gas Hydrate Stratigraphic Test Well, Alaska North Slope: Implications of uncertainties. Mar. Pet. Geol. 28, 517–534. https://doi.org/10.1016/j.marpetgeo.2010.01.005

Nandanwar, M.S., Anderson, B.J., Ajayi, T., Collett, T.S., Zyrianova, M.V., 2016. Evaluation of gas production potential from gas hydrate deposits in National Petroleum Reserve Alaska using numerical simulations. J. Nat. Gas Sci. Eng. 36, 760–772. https://doi.org/10.1016/j.jngse.2016.11.021

Pooladi-Darvish, M., Hong, H., 2011. Use of formation pressure test results over a hydrate interval for long-term production forecasting at the Mount Elbert Gas Hydrate Stratigraphic Test Well, Alaska North Slope: Implications of uncertainties. Mar. Pet. Geol. 28, 535–545. https://doi.org/10.1016/j.marpetgeo.2010.01.006

Reagan, M.T., Kowalsky, M.B., Moridis, G.J., Silpngarmlert, S., 2010. The Effect of Reservoir Heterogeneity on Gas Production From Hydrate Accumulations in the Permafrost. Presented at the SPE Western Regional Meeting, Anaheim, California, U.S.A.

Riedel, M., Willoughby, E.C., Chopra, S. (Eds.), 2010. Geophysical Characterization of Gas Hydrates. Society of Exploration Geophysicists. https://doi.org/10.1190/1.9781560802197

Sloan, E.D., 2003. Fundamental principles and applications of natural gas hydrates. Nature 426, 353–363. https://doi.org/10.1038/nature02135

Sloan, E.D., Koh, C., 2007. Clathrate Hydrates of Natural Gases, Third Edition. CRC Press.

Stone, H.L., 1970. Probability Model for Estimating Three-Phase Relative Permeability. J. Pet. Technol. 22, 214–218. https://doi.org/10.2118/2116-PA

Tamaki, M., Fujii, T., Suzuki, K., 2017. Characterization and Prediction of the Gas Hydrate Reservoir at the Second Offshore Gas Production Test Site in the Eastern Nankai Trough, Japan. Energies 10, 1678. https://doi.org/10.3390/en10101678

van Genuchten, M.Th., 1980. A Closed-form Equation for Predicting the Hydraulic Conductivity of Unsaturated Soils. Soil Sci. Soc. Am. J. 44, 892. https://doi.org/10.2136/sssaj1980.03615995004400050002x

Waite, W.F., Santamarina, J.C., Cortes, D.D., Dugan, B., Espinoza, D.N., Germaine, J., Jang, J., Jung, J.W., Kneafsey, T.J., Shin, H., Soga, K., Winters, W.J., Yun, T.-S., 2009. Physical properties of hydrate-bearing sediments. Rev. Geophys. 47. https://doi.org/10.1029/2008RG000279

Walsh, M.R., Hancock, S.H., Wilson, S.J., Patil, S.L., Moridis, G.J., Boswell, R., Collett, T.S., Koh, C.A., Sloan, E.D., 2009. Preliminary report on the commercial viability of gas production from natural gas hydrates. Energy Econ. 31, 815–823. https://doi.org/10.1016/j.eneco.2009.03.006

Wilson, S.J., Hunter, R.B., Collett, T.S., Hancock, S., Boswell, R., Anderson, B.J., 2011. Alaska North Slope regional gas hydrate production modeling forecasts. Mar. Pet. Geol. 28, 460–477. https://doi.org/10.1016/j.marpetgeo.2010.03.007

Winters, W., Walker, M., Hunter, R.B., Collett, T.S., Boswell, R., Rose, K., Waite, W., Torres, M., Patil, S., Dandekar, A., 2011. Physical properties of sediment from the Mount Elbert Gas Hydrate Stratigraphic Test Well, Alaska North Slope. Mar. Pet. Geol. 28, 361–380. https://doi.org/10.1016/j.marpetgeo.2010.01.008

Yan, C., Li, Y., Cheng, Y., Wang, W., Song, B., Deng, F., Feng, Y., 2018. Sand production evaluation during gas production from natural gas hydrates. J. Nat. Gas Sci. Eng. 57, 77–88. https://doi.org/10.1016/j.jngse.2018.07.006

Yu, M., Li, W., Jiang, L., Wang, X., Yang, M., Song, Y., 2018. Numerical study of gas production from methane hydrate deposits by depressurization at 274K. Appl. Energy, Transformative Innovations for a Sustainable Future – Part III 227, 28–37. https://doi.org/10.1016/j.apenergy.2017.10.013

Yuan, Y., Xu, T., Xin, X., Xia, Y., 2017. Multiphase Flow Behavior of Layered Methane Hydrate Reservoir Induced by Gas Production. Geofluids 2017, 1–15. https://doi.org/10.1155/2017/7851031

Zheng, R., Li, S., Li, X., 2018. Sensitivity analysis of hydrate dissociation front conditioned to depressurization and wellbore heating. Mar. Pet. Geol. 91, 631–638. https://doi.org/10.1016/j.marpetgeo.2018.01.010